Journal of Catalysis **183,** 355–367 (1999)
Article ID jcat.1999.2401, available online at http://www.idealibrary.com on IDEAL®

Kinetics of Hydrogen–Deuterium Exchange Reactions of Methane and Deuterated Acid FAU- and MFI-Type Zeolites

Bart Schoofs, Johan A. Martens, Pierre A. Jacobs, and Robert A. Schoonheydt[1]

Centrum voor Oppervlaktechemie en Katalyse (C.O.K.), Faculteit Landbouwkundige en Toegepaste Biologische Wetenschappen, Katholieke Universiteit Leuven, Kardinaal Mercierlaan 92, B-3001 Heverlee, Belgium

Received October 21, 1998; revised December 18, 1998; accepted December 21, 1998

The kinetics of the consecutive H–D exchange reactions between methane and deuterated acid FAU- and MFI-type zeolites was studied with on-line mass spectrometric product analysis, in the temperature range 450 to 550°C. On both zeolite types, the rate constant of H–D exchange increases with decreasing Al content. At the same Al content, the reaction rate constant of MFI is ca. three times larger than that of FAU, showing that chemical composition and structural effects are important in determining the rate of exchange. The apparent activation energy is in the range 122–150 kJ/mol, independent of the Al content and structure type. A kinetic isotope effect of approximately 1.7 was found, which is in disagreement with the earlier proposed concerted reaction mechanism (G. J. Kramer, R. A. van Santen, C. A. Emeis, and A. K. Nowak, *Nature* **363, 529, 1993).**

Key Words: **H–D exchange; methane; acid zeolites.**

INTRODUCTION

Bridging hydroxyl groups of the type Al–OH–Si are the active sites of acid zeolite catalysts (2–4). The Brønsted acid strength of these bridging hydroxyls is dependent on the structure type and framework composition. Thus, maximum acid strength is reached when the bridging hydroxyl is isolated, i.e., without Al atoms being present in next-nearest-neighbor (NNN) positions in the framework (5, 6).

This NNN principle is based on spectroscopic and catalytic observations. The O_1–H stretching vibration in FAU zeolites is shifted from 3660 cm^{-1} for a Si/Al ratio of 1.25 to 3610 cm^{-1} for Si/Al ratios $\geq$8, and the ^{1}H chemical shift from 4.0 to 4.7 ppm (7, 8). These changes are thought to reflect the increase in acid strength with increasing Si/Al ratio. In the cracking of hexane over a series of dealuminated Y zeolites, maximum activity is obtained for a zeolite with 30 Al atoms per unit cell or a Si/Al ratio of 5.4 (9, 10). In the cracking of hexane over ZSM-5, the activity per site is constant over a wide range, reflecting the uniformity of the acid sites when they are highly diluted in the zeolite (11).

Over the last few years, H–D exchange reactions of small alkanes have been used to gain insight into the mechanisms of alkane conversions over acid zeolites (12–17). Two essentially different reaction mechanisms have been proposed. The bimolecular route consists of a hydride transfer from the incoming alkane to an adsorbed alkyl carbenium ion (18, 19). In the monomolecular route, a proton is added to the alkane, with the formation of an alkyl carbonium ion (20–23).

Hydrogen–deuterium exchange between methane and an acid zeolite is a model reaction that attracted much attention from a theoretical viewpoint (24, 25). A concerted reaction mechanism was proposed (1, 26), in which the hydrogen atom of the bridging hydroxyl group moves towards the methane carbon atom, while at the same time, a deuterium atom from methane (CD_4) moves towards an oxygen atom of the zeolite. The reaction coordinate is almost along the lines connecting the O–H–C and C–D–O atoms. The transition state is obtained when the H and D atoms are halfway between the oxygen and carbon atoms. Using this transition state and a H_3Si–O–$Al(OH)_2$–OH–SiH_3 cluster, representing the zeolite, the activation energy for the reaction was calculated to be 150 ± 20 kJ/mol. The exchange rate was theoretically predicted using Eyring's transition state theory and found to be in reasonable agreement with the experimental rates determined with *in situ* infrared spectroscopy.

When the transition state of the concerted reaction mechanism is frozen into the FAU and MFI structures, the influence of chemical composition (Si/Al ratio) and structure (MFI vs FAU) can be studied with the electronegativity equalization method (EEM) (27, 28). This is a semiempirical density functional (DFT) method that requires two parameters for each atom type and exact knowledge of the structure, i.e., the coordinates of the atoms in the structure. They can be generated by the distance-least-squares (DLS) method. It follows from these calculations that Al in NNN positions hampers the reaction and that the influence of Al

[1] To whom correspondence should be addressed. Fax: +32–16–32 19 98. E-mail: robert.schoonheydt@agr.kuleuven.ac.be.

0021-9517/99 $30.00

content or chemical composition is more important by one order of magnitude than that of structure type (29, 30).

In this paper the H–D exchange reaction between methane and deuterated FAU- and MFI-type zeolites was studied experimentally in a recirculation reactor using on-line monitoring of the reaction products with a mass spectrometer. The goals of this study were to establish structural (FAU vs MFI) and chemical (Si/Al ratio) effects on the reaction kinetics and to validate results of the theoretical calculations based on a concerted reaction mechanism.

EXPERIMENTAL METHODS

Zeolites

The USY-type zeolites CBV712, CBV720, and CBV780 and the ZSM-5 zeolites CBV3020, CBV5020, and CBV8020 were from PQ (Table 1) and used as received. A detailed characterization of these samples is provided by Remy *et al.* (31). The sample Y1 was from Zeocat; the Y2 sample was a gift from Exxon Chemical Europe.

The number of acid sites on dry zeolite weight basis was calculated from the Si/Al ratios of Table 1, assuming all Al atoms to be in lattice positions, except when stated differently. Zeolite samples in NH_4^+ and H^+ form were used as such. NH_4^+ exchange of the Na^+ zeolites was performed in NH_4Cl solutions with 10-fold excess of NH_4^+ with respect to the cation exchange capacity at a solid : liquid ratio of 1 g/dm^3. The samples were exchanged overnight under continuous stirring and washed with bidistilled water until Cl^- free. The procedure was repeated three times, to ensure maximum exchange. After washing, the samples were dried at 60°C and stored over a saturated $CaCl_2$ solution.

For the catalytic experiments, the proton and ammonium exchanged zeolites were activated in an oxygen flow at 500°C for 8 h. The heating rate was 4°C per minute.

TABLE 1

Characterization of the Zeolites

Sample	Code[a]	Topology	Si/Al	No. of sites[b] (mmol g^{-1})
H-ZSM-5	CBV 3020	MFI	16.5	0.952
H-ZSM-5	CBV 5020	MFI	25.0	0.641
H-ZSM-5	CBV 8020	MFI	39.0	0.417
H-ZSM-5	CBV 1502	MFI	77.5	0.212
H-Y	Y1	FAU	2.71	4.492
H-Y	Y2	FAU	3.6	3.623
USY	CBV 712	FAU	5.45	2.584
USY	CBV 720	FAU	13.49	1.150
USY	CBV 780	FAU	36.9	0.440

[a] Commercial code name or designation.
[b] Corresponding to the number of Al atoms.

H–D Exchange Experiments

The catalytic experiments were performed in a recirculation reactor, connected via a variable leak to a MD800 mass spectrometer from Interscience. The capillary leak is constructed from an inox tubing with an internal diameter of 0.01 in. The flow through the capillary was adjusted to 0.6 ml min^{-1} with a needle valve at the beginning of the transfer line. The capillary leak is situated in the center of the batch volume to ensure representative sampling. The capillary is heated to 120°C and flushed with He to remove all traces of molecules (mainly adsorbed water) that might interfere with detection of the methane isotopomers. By switching the transfer line between the reactor and the He feed, it was found that the response time of the transfer line was only a few seconds.

When the catalyst is brought into the reactor, it is first deuterated with a D_2O saturated He flow at 200°C for 120 min. After deuteration, all remaining water was removed by calcining the sample in a He flow at 500°C for 1 h. The catalyst was then brought to reaction temperature and the reactor was evacuated. After evacuation, the desired amounts of helium and methane were added. The amount of methane was controlled via its partial pressure in the reactor. All experiments were performed at a total pressure of 1000 mbar. The reactor was first operated in bypass mode, to obtain a good mixture of methane and helium. During this bypass operation, there was no contact between methane and the catalyst. This allowed determination of the background signal (mainly H_2O at $m/z = 18$ and $m/z = 17$) and the methane fragmentation pattern. This fragmentation pattern was necessary for further analysis of the experimental data. The gas mixture was circulated by a membrane pump at the rate of 2 liters min^{-1} to ensure complete mixing of reagents and products.

Five reaction temperatures between 450 and 550°C were chosen, together with three methane concentrations between 0.5 and 2% methane in helium. The methane concentration was kept under 2% to keep the amount of methane hydrogen atoms at the same order of magnitude as the amount of deuterium atoms present on the zeolite surface. The upper limit of the reaction temperature was set by the onset of methane pyrolysis and the lower temperature limit by the duration of the experiment. At a leak rate of 0.6 ml/min and a total reactor volume of 1340 ml, the total duration of the experiment should not be longer than 200 min, to keep the amount of products lost for analysis under 10% of the initial amount. During the reaction, the $m/z = 2$–50 range was scanned with a scan time of 0.45 s and a delay of 9.55 s between two successive scans.

The infrared measurements were performed on a Nicolet 730 FT-IR spectrometer, equipped with a DTGS detector and 100 scans were accumulated for one spectrum at a resolution of 0.9 cm^{-1}. The samples were pressed into thin self-supporting wafers and placed in the high-temperature

IR cell. This IR cell with CaF_2 windows allows measurements at temperatures up to 580°C. The sample can be exposed to different gases and the cell can also be evacuated.

RESULTS

Deuteration of the Zeolites

To make H exchange reactions accessible to experimental investigation, it is necessary to label the reactant or the catalyst with deuterium. When the fragmentation of the reactant molecule has to be taken into account, it is often easier to use deuterated catalysts. For example in the case of the H exchange of methane with a deuterated catalyst, the isotopomers of methane at $m/z = 16$–20 can be monitored without interference of the fragmentation peaks at $m/z = 12$–15. When deuterated methane is used instead, elaborate corrections are necessary to make the distinction between the molecular ion peaks of the different isotopomers and the intense fragmentation peaks at $m/z = 16$ and $m/z = 18$.

The deuteration is based on a procedure described by Mota *et al.* (20). It gives samples that are fully deuterated without loss of framework Al or crystallinity. This was verified with infrared spectroscopy. The OH stretching vibrations of the bridging hydroxyl groups and the silanol groups (3500–3800 cm^{-1} region) decrease progressively, while new absorption bands grow in the 2600–2800 cm^{-1} region. These new bands are the O–D stretching vibrations of the bridging hydroxyl and silanol groups. When, after 60 min, the O–H stretching vibrations have disappeared, complete deuteration has been achieved.

Subsequently, the sample was contacted with a mixture of 2% CH_4 in N_2 at 500°C and at given times, the IR cell was evacuated and a spectrum was recorded. This allows the reaction of CH_4 with the surface O–D groups to be monitored and the results of this experiment are shown in Fig. 1. As the contact time between the zeolite and methane increases, O–H stretching vibrational bands are formed at 3550, 3630, and 3740 cm^{-1}, while the O–D bands gradually decrease at 2620, 2670, and 2750 cm^{-1}. Thus, bridging hydroxyl groups (2620 and 2670 cm^{-1}) as well as silanol groups (2750 cm^{-1}) are available for H–D exchange with methane.

H–D Exchange Kinetics

Spectral corrections. The isotopomers of methane, $CH_{4-x}D_x$ with $x = 0$–4, have their own characteristic fragmentation patterns, which overlap each other. To obtain the pure molecular ion peaks of the methane isotopomers, corrections have to be made for the fragmentation peaks that contribute to the m/z signals.

The reactant, methane in He, is run over a bypass to determine its fragmentation pattern (Eq. [7]). With this pattern and with the hypothesis that the degree of fragmentation of the isotopomers is identical, Eqs. [1]–[6] are obtained, relating mass spectrometer signals to concentrations:

$$[CD_4] = [m/z = 20], \quad [1]$$

$$[CD_3H] = [m/z = 19], \quad [2]$$

$$[CD_2H_2] = [m/z = 18] - F_1 \cdot [CD_4] - \tfrac{1}{4} \cdot F_1 \cdot [CD_3H], \quad [3]$$

$$[CDH_3] = [m/z = 17] - \tfrac{3}{4} \cdot F_1 \cdot [CD_3H] - \tfrac{1}{2} \cdot F_1 \cdot [CD_2H_2], \quad [4]$$

$$[CH_4] = [m/z = 16] - F_2 \cdot [CD_4] - \tfrac{1}{2} \cdot F_2 \cdot [CD_3H] - \tfrac{1}{6} \cdot F_2 \cdot [CD_2H_2] - \tfrac{1}{2} \cdot F_1 \cdot [CD_2H_2] - \tfrac{3}{4} \cdot F_1 \cdot [CDH_3], \quad [5]$$

$$[m/z = 15]_{corr} = [m/z = 15] - \tfrac{1}{2} \cdot F_2 \cdot [CD_3H] - \tfrac{2}{3} \cdot F_2 \cdot [CD_2H_2] - \tfrac{1}{2} \cdot F_2 \cdot [CDH_3] - \tfrac{1}{4} \cdot F_1 \cdot [CDH_3] - F_1 \cdot [CH_4], \quad [6]$$

in which

$$\frac{[m/z = 15]}{[m/z = 16]} = \text{loss of one proton} = F_1 \quad \text{and}$$
$$\frac{[m/z = 14]}{[m/z = 16]} = \text{loss of two protons} = F_2. \quad [7]$$

The application of these equations gives the disappearance of CH_4 and the formation of CH_3D, CH_2D_2, CHD_3, and CD_4 as a function of time. This type of correction can also be extended to the $m/z = 15$ signal. Obviously, the resulting $[m/z = 15]_{corr}$ will approximate zero, since it consists entirely of fragmentation peaks. The approach of the corrected $m/z = 15$ signal to zero is an indication for the quality of the correction. In our experiments, the absolute intensity of the corrected $m/z = 15$ signal was always less than 5% of the original $m/z = 15$ signal, confirming the validity of the proposed data treatment.

Kinetic analysis. Initially, the rate of transfer of deuterium from the zeolite to methane equals the rate of H exchange, since every exchange reaction results in the transfer of one deuterium atom. After some time, however, the deuterium atoms that are now present on the methane will also exchange. The exchange of deuterium on methane with deuterium on the zeolite cannot be observed. Exchange of deuterium of methane with a proton of the zeolite leads even to a deuterium transfer from methane to the zeolite. Thus, while the overall exchange rate remains constant, the apparent deuterium transfer rate will decrease with time and eventually become zero when equilibrium is achieved.

The hydrogen exchange reaction between methane and an acid zeolite and the general form of the rate equation are expressed in Eq. [8] (Y represents the zeolite). Similarly, for the hydrogen–deuterium exchange reaction

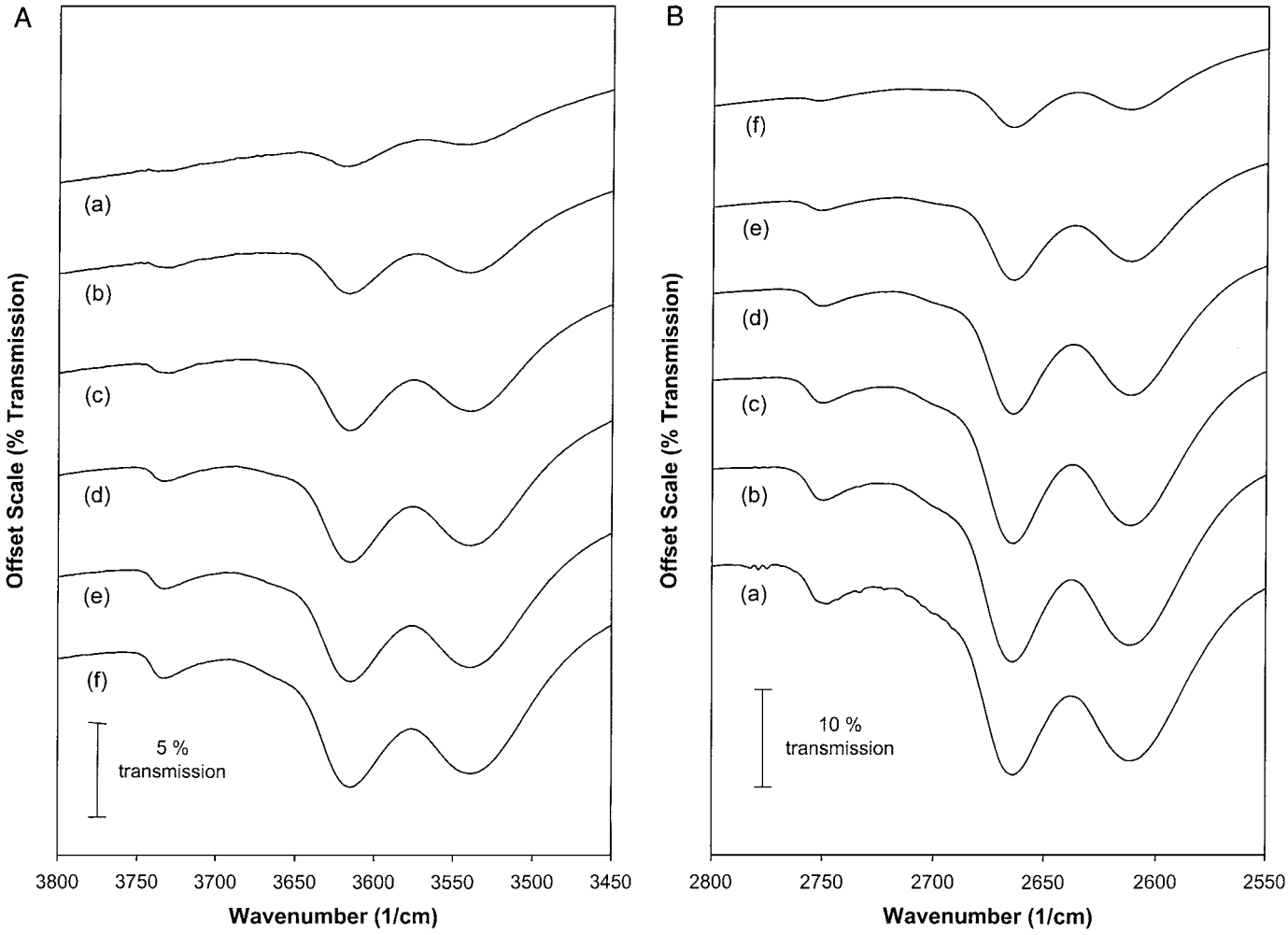

FIG. 1. Infrared spectra for the H–D exchange reaction between the hydroxyl groups of a FAU type zeolite with Si/Al = 3.6 and 2% methane in N_2 at 500°C: (A) O–H stretching frequency region and (B) O–D stretching frequency region, after (a) 0 min, (b) 15 min, (c) 60 min, (d) 180 min, (e) 450 min, and (f) 1150 min.

between methane and a deuterated zeolite, the initial reaction and the exchange rate R can be written as in Eq. [9]. At any given time t after the start of the reaction, the overall exchange rate R is made up of the sum of the exchange rates of 16 subreactions that are all occurring at their own specific rates. These 16 subreactions with their respective rate expressions, R_1–R_{16}, are presented in the Appendix.

$$CH_4 + HY \leftrightarrow CH_4 + HY, \quad R = k \cdot [HY]^x [CH_4]^y, \qquad [8]$$

$$CH_4 + DY \leftrightarrow CH_3D + HY, \quad R = k \cdot [DY_{in}]^x [CH_{4in}]^y. \qquad [9]$$

In Eqs. [8] and [9], k is the rate constant and the exponents x and y are the orders of the reaction. No prior knowledge of the order of the reaction or the rate constant is required to perform the kinetic analysis that is described hereafter.

Experimentally only the transfer of deuterium from the zeolite to methane can be observed. The amount of deuterium X transferred from the zeolite to methane at time t equals the total amount of deuterium present on the methane or the total amount of hydrogen present on the zeolite (Eq. [10]). The mathematical expression for the transfer of deuterium from the zeolite to the methane fraction, in terms of the rates of the 16 subreactions, is presented in Eq. [11], which can be converted to Eq. [12] (see Appendix).

$$X = [CH_3D] + 2[CH_2D_2] + 3[CHD_3] + 4[CD_4] = [HY], \qquad [10]$$

$$\frac{d[HY]}{dt} = R_9 + R_{10} + R_{12} + R_{14} - R_2 - R_4 - R_6 - R_8, \qquad [11]$$

$$\frac{d([HY]/4[CH_{4in}])}{dt} = R \cdot \frac{1}{4[CH_{4in}]} \cdot \frac{4[CH_{4in}] + [DY_{in}]}{[DY_{in}]} \cdot \left(\frac{[DY_{in}]}{4[CH_{4in}] + [DY_{in}]} - \frac{[HY]}{4[CH_{4in}]} \right). \qquad [12]$$

In these equations, $[CH_{4in}]$ is the initial methane

concentration and $[DY_{in}]$ the initial deuterium concentration. In practice, it is easier to work with fractions (Φ). They are defined in Eqs. [14] and [15], where Φ_{eq} is the equilibrium fraction. When $\ln(\Phi_{eq} - \Phi)$ is plotted versus time, a straight line is obtained and R can be calculated from the slope (Eq. [16]).

$$\frac{d\Phi}{dt} = \frac{R}{4[CH_{4in}] \cdot \Phi_{eq}} \cdot (\Phi_{eq} - \Phi) \quad [13]$$

$$\Phi = \frac{[CH_3D] + 2[CH_2D_2] + 3[CHD_3] + 4[CD_4]}{4[CH_{4in}]} = \frac{[HY]}{4[CH_{4in}]}, \quad [14]$$

$$\Phi_{eq} = \frac{[DY_{in}]}{4[CH_{4in}] + [DY_{in}]}, \quad [15]$$

$$\ln\left(\frac{\Phi_{eq} - \Phi}{\Phi_{eq}}\right) = \frac{-R}{4[CH_{4in}] \cdot \Phi_{eq}} \cdot t. \quad [16]$$

H–D exchange rates and apparent activation energies. The results of an experiment with a mixture of 0.5% methane in helium and 1.5 g of a CBV5020 (H-ZSM-5 with Si/Al = 25) catalyst at 500°C are presented in Fig. 2. It shows the evolution with time of the $m/z = 16$–20 signals. After spectral correction (Eqs. [1]–[7]) Fig. 3 is obtained. The methane signal decreases with time and gives rise to consecutive formation of deuterated products. The overall exchange rate can be calculated from the slope of the straight line that is obtained when $\ln(\Phi_{eq} - \Phi)$ is plotted versus time (Fig. 4). The exchange rate per site is obtained by dividing the overall exchange rate by the number of sites, which is defined as the number of Al atoms, assuming that all Al is in the lattice.

To correlate these reaction rate data with the zeolite properties, it is necessary to verify the absence of any intermolecular H–D exchange of methane in the gas phase. Blank experiments in an empty reactor tube, performed with a 50 : 50 mixture of CH_4 and CD_4, showed that at temperatures up to 580°C no measurable exchange occurs between CH_4 and CD_4.

The exchange rates per site for a series of FAU-type zeolites with different Si/Al ratios are presented in Fig. 5 as a function of the Al/(Si + Al) ratio of the zeolites. The experiments were performed with a mixture of 1% CH_4 in He and temperatures of 450, 475, and 500°C. These data clearly indicate that the exchange rate per site decreases with increasing number of Al atoms per unit cell and tends to level off at low as well as at high Al content. When the same experiments are performed with a series of MFI-type zeolites (Fig. 6), the same trends are observed, but the leveling off takes place only at Al/(Al + Si) below 0.025 or Si/Al ratios above 40. For the most siliceous samples, the exchange rate per site even decreases below Al/(Si + Al) = 0.025. ZSM-5 samples with Si/Al ratios below 12 were not available to verify the behavior at higher acid site densities.

The exchange rates for the MFI- and FAU-type catalysts at 500°C and 1% CH_4 in He are compared in Fig. 7. These data show that at the same Al/(Si + Al) ratio, the exchange rate for MFI-type zeolites is higher than that for FAU-type

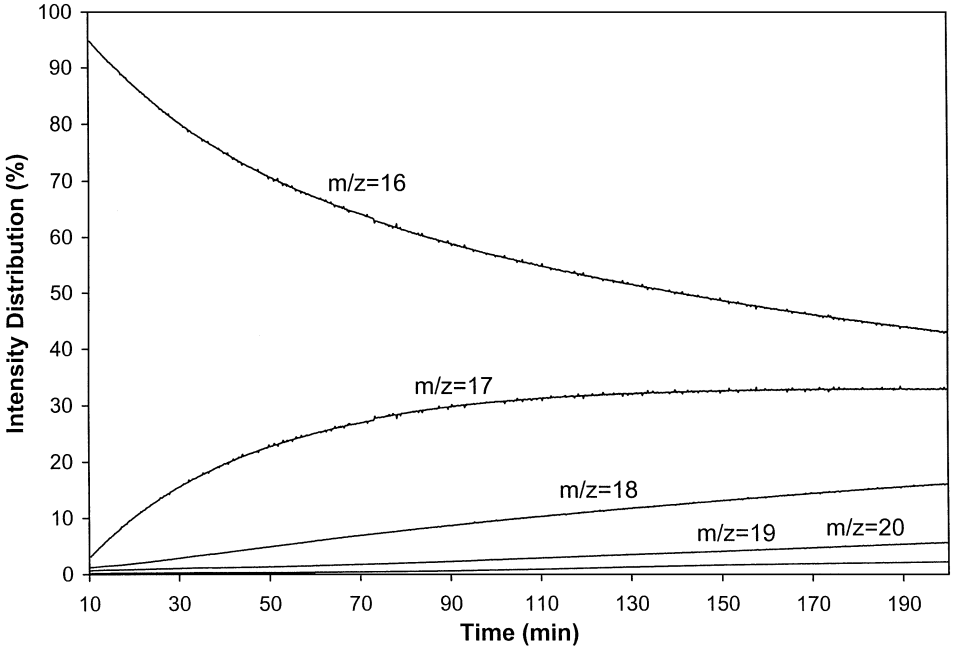

FIG. 2. Intensity distribution (%) of the m/z signals 16 to 20 for an experiment on a MFI-type zeolite with Si/Al = 25 and 0.5% CH_4 in He at 500°C.

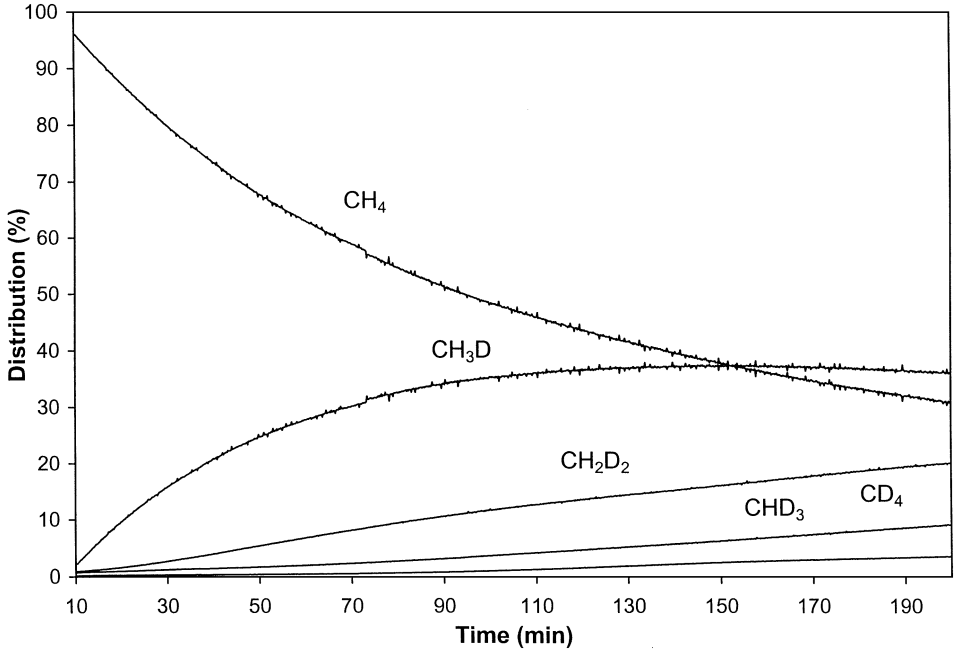

FIG. 3. Distribution of the methane isotopomers (%) as a function of time for an experiment on a MFI-type zeolite with Si/Al = 25 and 0.5% CH_4 in He at 500°C.

zeolites. This indicates that structure is important in determining the activity per site.

Remy *et al.* made a quantitative analysis of the different Al species in the FAU samples by ^{29}Si and ^{27}Al MAS NMR. They considered the following Al species: Al(IV) or tetrahedral framework Al, Al(VI) or octahedral extra-framework Al; Al(x) is an Al species that belongs to the framework and Al(I) is NMR-invisible Al, which accounts for the difference in Al content determined by chemical analysis and ^{27}Al NMR. If bridging hydroxyls are associated with Al(IV) only, as determined by NMR, than the activity per site is higher as shown by the full triangles of Fig. 7. However, the general trend of an increase in activity with decreasing Al/(Si + Al) ratio remains valid.

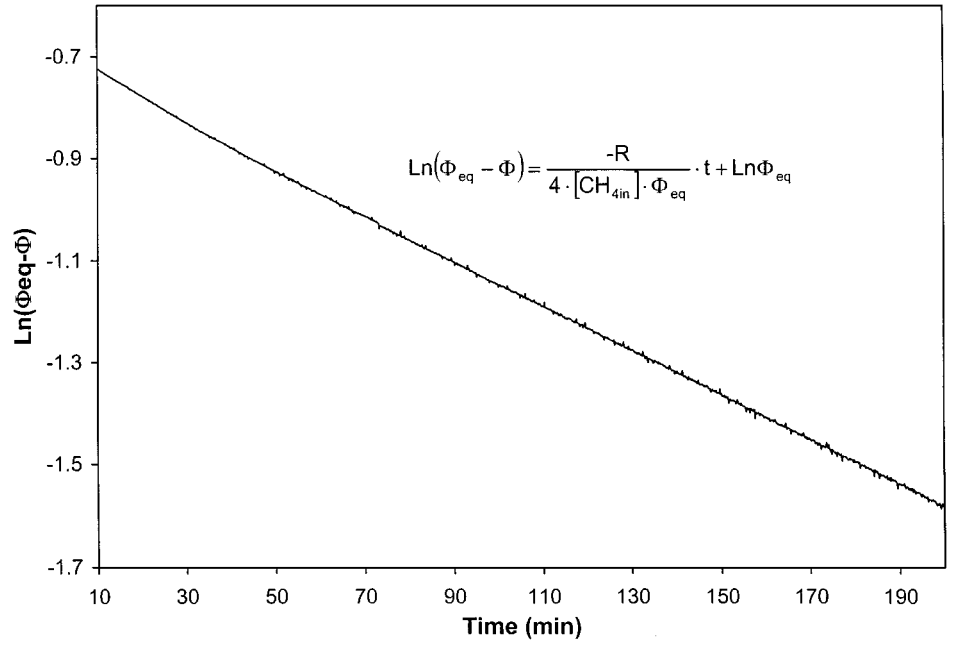

FIG. 4. Logarithmic plot of $\Phi_{final} - \Phi$ versus time; the exchange rate can be calculated from the slope of the straight line.

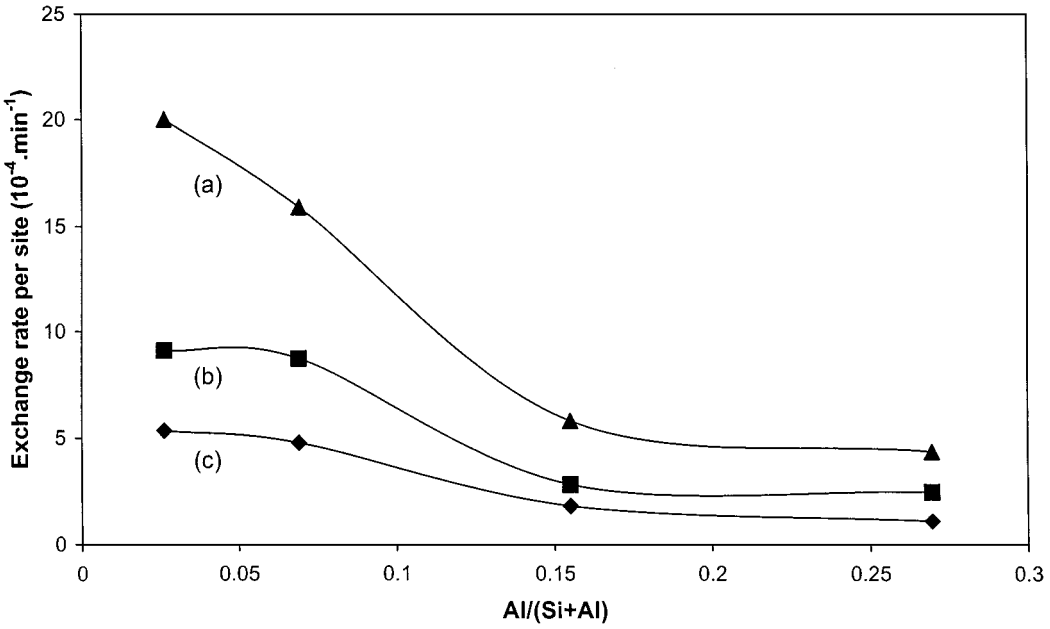

FIG. 5. Effect of Al content on the exchange rate for FAU-type zeolites; experiments were performed with 1% methane in helium at (a) 500°C, (b) 475°C, and (c) 450°C.

For both FAU- and MFI-type zeolites, experiments were performed with 1% CH_4 in He and temperatures ranging from 450 to 550°C. Ln(k) was plotted versus $1/T$ in an Arrhenius plot and the apparent activation energy for the H–D exchange reaction was calculated using the Arrhenius equation. The experimental values for the apparent activation energy were found to be in the range of 122–150 kJ/mol (Table 2), whatever the type of the zeolite and the Si/Al ratio. To obtain the true activation energy, the adsorption energy of methane, which is around −15 kJ/mol on both FAU and MFI type zeolites (32–34), has to be accounted for. This results in a true activation energy of 137–165 kJ/mol.

In addition, experiments were performed using deuterated methane (CD_4) and a H^+-zeolite. Now, the decrease in the amount of CD_4 ($m/z = 20$) and the increase in CHD_3, CH_2D_2, CH_3D, and CH_4 signals is followed as a function

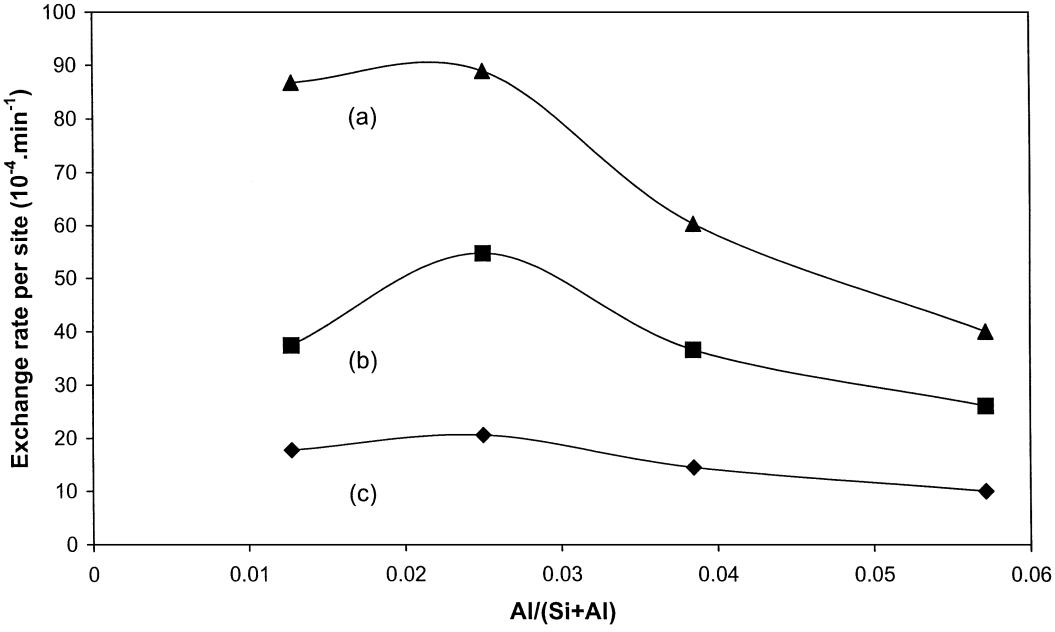

FIG. 6. Effect of Al content on the exchange rate for MFI-type zeolites; experiments were performed with 1% methane in helium at (a) 500°C, (b) 475°C, and (c) 450°C.

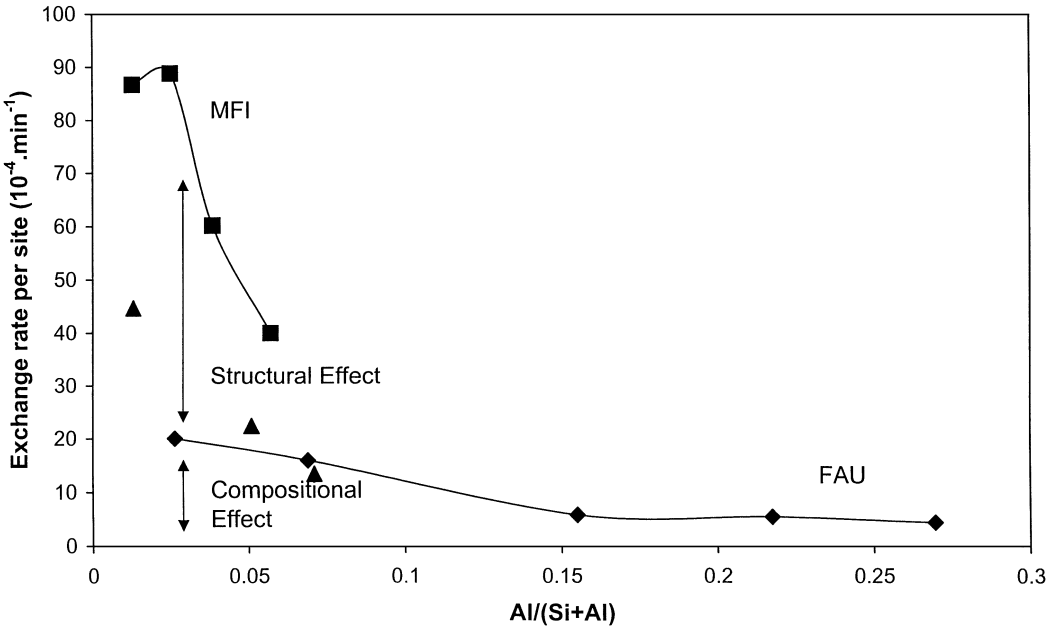

FIG. 7. Comparison of the exchange rates for FAU- and MFI-type zeolites with an indication of the structural and compositional effects; experiments were performed at 500°C with 1% methane in helium. Based on ^{27}Al NMR measurements [Ref. (30)], the data for CBV712, CBV720, and CBV780 were recalculated, taking into account tetrahedral Al only.

of time. The experimental data are treated analogously to those of the exchange between CH_4 and D^+-zeolites. The results show that the exchange rate with CD_4 is higher than that of CH_4. This is indicative for a kinetic isotope effect, represented as k_H/k_D, where k_H is the rate constant for the exchange between CD_4 and H^+-zeolites and k_D is the rate constant for the exchange between CH_4 and D^+-zeolites. The ratio k_H/k_D for MFI-type zeolites is 1.6–1.7 (Table 3).

Modeling of the Reaction Kinetics

The H–D exchange between methane and Brønsted acid sites can be modeled by a consecutive reaction ($CH_4 \rightarrow CH_3D \rightarrow CH_2D_2 \rightarrow CHD_3 \rightarrow CD_4$). A consecutive mechanism implies that the adsorption and desorption are fast compared with the exchange reaction. A single methane molecule will adsorb and desorb multiple times before it will undergo an exchange reaction.

TABLE 2

Apparent Activation Energy for the H–D Exchange of Methane on Some FAU- and MFI-Type Zeolites (kJ/mol)

MFI		FAU	
Si/Al	$E_{A,app}$ (kJ/mol)	Si/Al	$E_{A,app}$ (kJ/mol)
16.5	129	2.7	136
25	133	5.5	150
39	137	13.5	140
78	148	36.9	122

The model uses the 16 possible exchange reactions between methane and the zeolite as a starting point (see Appendix). These 16 reactions are subdivided into five groups, representing the five different isotopomers of methane, based on whether they take part in the formation or disappearance of that respective isotopomer. Using the rate equations of the 16 subreactions, one obtains a system of five differential equations, representing the formation and disappearance of the five isotopomers. For example in the case of the isotopomer CH_3D, $d[CH_3D]/dt = -R_2 + R_4 + R_9 - R_{10}$. These equations can be converted to Eqs. [17]–[21]:

$$\frac{d[CH_4]}{dt} = \frac{R}{[CH_{4in}][DY_{in}]}\left(\tfrac{1}{4}[CH_3D]^2 + \tfrac{1}{2}[CH_3D][CH_2D_2] + \tfrac{3}{4}[CH_3D][CHD_3] + [CH_3D][CD_4] - [DY_{in}][CH_4] + [CH_4][CH_3D] + 2[CH_4][CH_2D_2] + 3[CH_4][CHD_3] + 4[CH_4][CD_4]\right), \quad [17]$$

TABLE 3

Isotope Effect for MFI-Type Zeolites[a]

Si/Al	16.5	25	39
k_H/k_D	1.6	1.7	1.7

[a] k_H = rate constant for the exchange between CD_4 and H^+ zeolites and k_D = rate constant for the exchange between CH_4 and D^+ zeolites.

$$\frac{d[CH_3D]}{dt} = \frac{R}{[CH_{4in}][DY_{in}]}\big([CH_2D_2]^2 + \tfrac{3}{2}[CH_2D_2][CHD_3] + 2[CH_2D_2][CD_4] + [DY_{in}][CH_4] - [CH_4][CH_3D] - 2[CH_4][CH_2D_2] - 3[CH_4][CHD_3] - 4[CH_4][CD_4] - \tfrac{3}{4}[DY_{in}][CH_3D] + \tfrac{1}{2}[CH_3D]^2 + \tfrac{3}{2}[CH_3D][CH_2D_2] + \tfrac{3}{2}[CH_3D][CHD_3] + 2[CH_3D][CD_4]\big), \quad [18]$$

$$\frac{d[CH_2D_2]}{dt} = \frac{R}{[CH_{4in}][DY_{in}]}\big(\tfrac{9}{4}[CHD_3]^2 + 3[CHD_3][CD_4] + \tfrac{3}{4}[DY_{in}][CH_3D] - \tfrac{3}{4}[CH_3D]^2 - \tfrac{3}{2}[CH_3D][CH_2D_2] - \tfrac{3}{2}[CH_3D][CHD_3] - 3[CH_3D][CD_4] - \tfrac{1}{2}[DY_{in}][CH_2D_2] + \tfrac{3}{2}[CH_2D_2][CHD_3]\big), \quad [19]$$

$$\frac{d[CHD_3]}{dt} = \frac{R}{[CH_{4in}][DY_{in}]}\big([CH_3D][CD_4] + 4[CD_4]^2 + \tfrac{1}{2}[DY_{in}][CH_2D_2] - \tfrac{1}{2}[CH_3D][CH_2D_2] - [CH_2D_2]^2 - \tfrac{1}{2}[CH_3D][CHD_3] - \tfrac{5}{2}[CH_2D_2][CHD_3] - \tfrac{3}{2}[CHD_3]^2 - \tfrac{1}{4}[DY_{in}][CHD_3] + [CHD_3][CD_4]\big), \quad [20]$$

$$\frac{d[CD_4]}{dt} = \frac{R}{[CH_{4in}][DY_{in}]}\big(\tfrac{1}{4}[DY_{in}][CHD_3] - \tfrac{1}{4}[CH_3D][CHD_3] - \tfrac{1}{2}[CH_2D_2][CHD_3] - \tfrac{3}{4}[CHD_3]^2 - [CH_3D][CD_4] - 2[CH_2D_2][CD_4] - 4[CHD_3][CD_4] - 4[CD_4]^2\big). \quad [21]$$

These equations were solved with the mathematical software package MAPLEV Release4, using a fourth- and fifth-order Runge–Kutta method.

For a boundary condition equivalent to an experiment with a CBV5020 and 0.5% methane, this system was solved and a graphical representation is given in Fig. 8. The results from the modeling correspond well with the experimental data, indicating that a consecutive exchange mechanism is a good model to describe the experimental data. The fact that a heterogeneous catalyzed H–D exchange reaction can be described with a simple model for a gas-phase reaction indicates that the reaction is the rate-determining step. That there is no single-step perdeuteration can also be seen from the low initial intensity of mass 20 in the chromatogram.

DISCUSSION

The Zeolites

The H–D exchange of methane on H-form zeolites is an acid-catalyzed reaction that neatly runs without side reactions in the temperature frame 450–550°C. Therefore, it is a good reaction to test structure–activity relationships and to

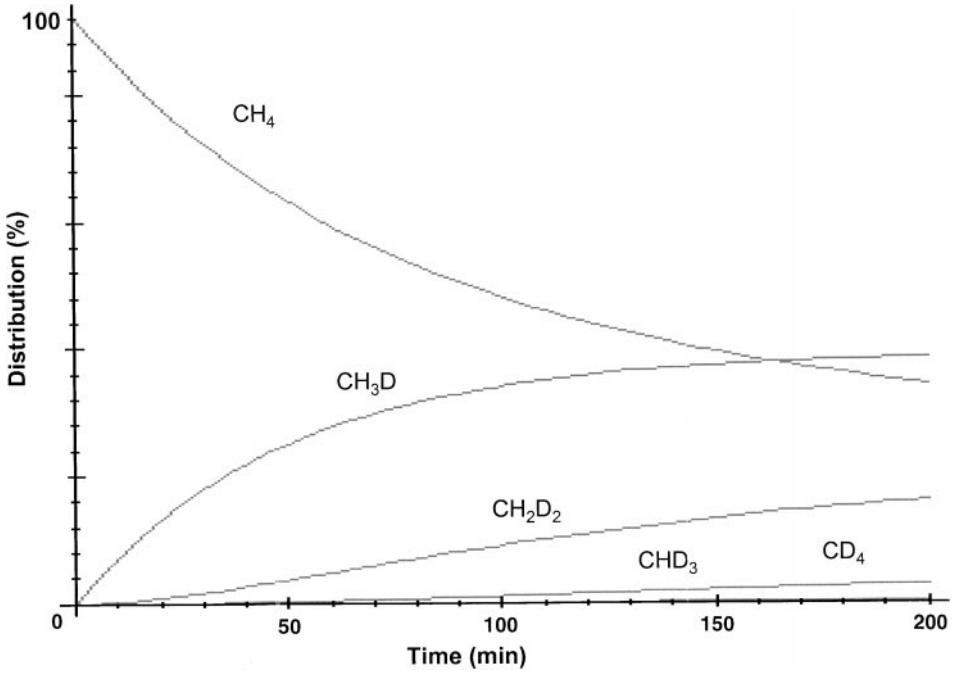

FIG. 8. Simulation of an experiment with a MFI-type zeolite with Si/Al = 25 and 0.5% methane in helium at 500°C.

experimentally observe the effects of chemical composition on activity. Ideally, this would require the use of "perfect" catalysts containing only bridging hydroxyls, all the Al in tetrahedral coordination in the lattice, no defects, and absence of silanols. Real catalysts contain some extra-lattice Al and defect sites such as silanols.

Silanol groups are considered weakly acidic or nonacidic. Do they take part in the reaction? Under the conditions of the present experiments, no exchange was observed on silica. However, in the IR cell, silanols of zeolites are deuterated and take part in the exchange reaction with methane (Fig. 1). Thus, either the silanols of silica have a different reactivity from those of zeolites, or under the exchange conditions the various hydroxyl groups form one pool of hydrogens on the surface.

Bridging hydroxyls are associated with structural Al, which is in tetrahedral coordination. Other types of Al might also be associated with hydroxyl groups. However, they are not well characterized and their acidity is unknown. We have therefore taken either the total Al content or the tetrahedral Al content to calculate the activity per site. The data on FAU in Fig. 7 indicate that the general trend of activity increase with decreasing Al/(Si + Al) ratio does not change. On the other hand, there is no correlation between the activity per site and the amount of extra-lattice Al, with an NMR signal characteristic of octahedral Al. It is concluded that the H–D exchange between CH_4 and deuterated zeolites is a Brønsted acid-catalyzed reaction. Total as well as tetrahedral Al can be used to estimate the number of active sites from which the activity per site is obtained.

Reaction Mechanism

The H–D exchange reaction is a stepwise reaction, wherein a CH_4 molecule exchanges one H at a time with the D of a bridging deuteroxyl group. Thus, CH_3D, CH_2D_2, CHD_3, and CD_4 are formed consecutively. Both the experimental results and the modeling confirm this picture. The transition state is a penta-coordinated carbonium ion with one H and one D in interaction with two neighboring oxygens of the zeolite lattice:

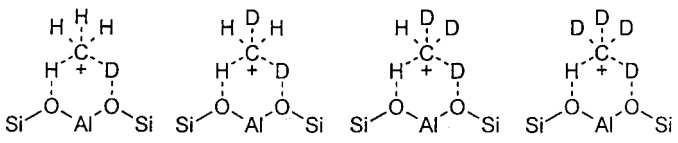

The experimental values of the activation energy (137–165 kJ/mol) are in good agreement with the theoretical value of 150 ± 20 kJ/mol that was calculated based on a concerted reaction mechanism. A concerted reaction mechanism means that the transition state of the reaction $CH_4 + \equiv Al{-}OD{-}Si\equiv$ is exactly the same as that of $CD_4 + \equiv Al{-}OH{-}Si\equiv$. This holds true if the following two hypotheses are valid: (1) the two oxygens of the lattice taking part in the reaction must be crystallographically equivalent; (2) the reaction coordinate contains the atoms O–D–C–H–O only. No kinetic isotope effect will be measured.

The experimentally observed kinetic isotope effect of 1.7 indicates that the concerted reaction mechanism is invalid. For a reaction in the FAU supercages the two structural oxygens taking part in the reaction are O_1 and O_4. Furthermore, the theoretically calculated intrinsic reaction coordinate contains a small contribution from the CH_3 fragment of methane (29). The reason for the theoretically proposed concerted mechanism is that in the theoretical calculations a mirror plane was imposed on the transition state (1, 26). When it is removed, preliminary calculations at the AM1 level show that the reaction does not occur via a concerted mechanism (35).

Structure–Activity Relationships

The ultimate goal of catalysis research is the establishment of the relation between structure and composition of a catalyst, on one hand, and activity and selectivity of the reaction it catalyzes, on the other hand. In the case of the H–D exchange of methane with acid zeolites, selectivity effects are absent and structure/composition–activity relationships can be discussed.

According to the NNN principle, a constant maximum activity per site is expected when the bridging hydroxyls or lattice Al are separated by at least two Si tetrahedra (5, 6, 29). Such a phenomenon is observed for MFI (Fig. 6) and for FAU (Fig. 5). For FAU, maximum activity is reached at a Si/Al ratio of about 15 or $Al/(Si + Al) = 0.06$. Such a value is in agreement with the NNN principle and the statement that Al atoms at a longer mutual distance have no significant influence on activity. For MFI, maximum activity per site is reached only at $Si/Al = 40$ or $Al/(Si + Al) = 0.024$.

If a random distribution of Al is assumed, the Si/Al ratios of 15 and 40 correspond to 1.2 and 2.2 nm^3/Al in the FAU and MFI frameworks, respectively. Thus, the distance between Al tetrahedra necessary to obtain a constant activity per site is larger in MFI than in FAU. This can be related to the higher T-atom density of MFI (17.9 T/1000 $Å^3$) than that of FAU (12.7 T/1000 $Å^3$) (36). The conclusion is that structure (density of T atoms) and chemical composition (NNN principle) determine the activity per site. The same parameters determine the acid strength of the bridging hydroxyls. Thus, both for FAU and for MFI the acid strength increases with decreasing Al/(Si + Al) ratio. The acid strength of the bridging hydroxyl of MFI is higher than that of the bridging hydroxyl in FAU. One can then use the activity per site in the H–D exchange as a measure of acidity of bridging hydroxyl groups.

Theoretical calculations tend to indicate that local properties of the active site are more important than long-range effects. Local properties are usually related to chemical

composition, long-range effects to structure. Our results show that chemical composition and structure are both important and cannot be separated.

To refine the relative importance of chemical composition and structure, additional experiments have to be designed to reveal the influence of silanol groups, defects, and impurities on the reaction under study. From the theoretical viewpoint powerful *ab initio* methods must be available to study structural effects. Up to now these structural effects can be taken into account with the EEM method only. However, one has to calculate theoretically a transition state and freeze it in the zeolite to perform such EEM calculations. Structure relaxation is not accounted for in the EEM calculations.

CONCLUSIONS

Both structure and composition determine the activity of the bridging hydroxyl group in the H–D exchange reaction with methane over acid aluminosilicate zeolites of FAU and MFI structure type. A composition effect is evidenced in the change of the activity per site with changing Al content. A constant and maximum activity per site is observed in FAU samples with Si/Al ratio exceeding 15, as predicted by the NNN principle. For MFI, constant activity is reached only at Si/Al above 40. The structural effect is evidenced by the much higher activity of a bridging hydroxyl in MFI than in FAU zeolites. The observed kinetic isotope effect is in disagreement with H–D exchange proceeding via a concerted reaction mechanism. The apparent activation energies of 122–150 kJ/mol, independent of structure and chemical composition, do agree with a previously reported theoretical value of 150 kJ/mol (1). The influence of silanol groups, defects, and impurities remains to be investigated in more detail to refine the presently observed composition and structure effects.

APPENDIX

Sixteen exchange reactions can occur between the bridging hydroxyl groups of a zeolite and the isotopomers of methane, CH_4, CH_3D, CH_2D_2, CHD_3, and CD_4. The respective rate equations can be expressed as fractions of the global exchange rate R. The global exchange rate R is the sum of the exchange rates of the 16 subreactions.

$$[HY] + [CH_4] \rightarrow [HY] + [CH_4]$$
$$R_1 = R \cdot \frac{[CH_4][HY]}{[CH_{4in}][DY_{in}]} \quad \text{[i]}$$

$$[HY] + [CH_3D] \rightarrow [DY] + [CH_4]$$
$$R_2 = R \cdot \frac{1}{4}\frac{[CH_3D][HY]}{[CH_{4in}][DY_{in}]} \quad \text{[ii]}$$

$$[HY] + [CH_3D] \rightarrow [HY] + [CH_3D]$$
$$R_3 = R \cdot \frac{3}{4}\frac{[CH_3D][HY]}{[CH_{4in}][DY_{in}]} \quad \text{[iii]}$$

$$[HY] + [CH_2D_2] \rightarrow [DY] + [CH_3D]$$
$$R_4 = R \cdot \frac{1}{2}\frac{[CH_2D_2][HY]}{[CH_{4in}][DY_{in}]} \quad \text{[iv]}$$

$$[HY] + [CH_2D_2] \rightarrow [HY] + [CH_2D_2]$$
$$R_5 = R \cdot \frac{1}{2}\frac{[CH_2D_2][HY]}{[CH_{4in}][DY_{in}]} \quad \text{[v]}$$

$$[HY] + [CHD_3] \rightarrow [DY] + [CH_2D_2]$$
$$R_6 = R \cdot \frac{3}{4}\frac{[CHD_3][HY]}{[CH_{4in}][DY_{in}]} \quad \text{[vi]}$$

$$[HY] + [CHD_3] \rightarrow [HY] + [CHD_3]$$
$$R_7 = R \cdot \frac{1}{4}\frac{[CHD_3][HY]}{[CH_{4in}][DY_{in}]} \quad \text{[vii]}$$

$$[HY] + [CD_4] \rightarrow [DY] + [CHD_3]$$
$$R_8 = R \cdot \frac{[CD_4][HY]}{[CH_{4in}][DY_{in}]} \quad \text{[viii]}$$

$$[DY] + [CH_4] \rightarrow [HY] + [CH_3D]$$
$$R_9 = R \cdot \frac{[CH_4][DY]}{[CH_{4in}][DY_{in}]} \quad \text{[ix]}$$

$$[DY] + [CH_3D] \rightarrow [HY] + [CH_2D_2]$$
$$R_{10} = R \cdot \frac{3}{4}\frac{[CH_3D][DY]}{[CH_{4in}][DY_{in}]} \quad \text{[x]}$$

$$[DY] + [CH_3D] \rightarrow [DY] + [CH_3D]$$
$$R_{11} = R \cdot \frac{1}{4}\frac{[CH_3D][DY]}{[CH_{4in}][DY_{in}]} \quad \text{[xi]}$$

$$[DY] + [CH_2D_2] \rightarrow [HY] + [CHD_3]$$
$$R_{12} = R \cdot \frac{1}{2}\frac{[CH_2D_2][DY]}{[CH_{4in}][DY_{in}]} \quad \text{[xii]}$$

$$[DY] + [CH_2D_2] \rightarrow [DY] + [CH_2D_2]$$
$$R_{13} = R \cdot \frac{1}{2}\frac{[CH_2D_2][DY]}{[CH_{4in}][DY_{in}]} \quad \text{[xiii]}$$

$$[DY] + [CHD_3] \rightarrow [HY] + [CD_4]$$
$$R_{14} = R \cdot \frac{1}{4}\frac{[CHD_3][DY]}{[CH_{4in}][DY_{in}]} \quad \text{[xiv]}$$

$$[DY] + [CHD_3] \rightarrow [DY] + [CHD_3]$$

$$R_{15} = R \cdot \frac{3}{4} \frac{[CHD_3][DY]}{[CH_{4in}][DY_{in}]} \quad \text{[xv]}$$

$$[DY] + [CD_4] \rightarrow [DY] + [CD_4]$$

$$R_{16} = R \cdot \frac{[CD_4][DY]}{[CH_{4in}][DY_{in}]} \quad \text{[xvi]}$$

$$R = R_1 + R_2 + R_3 + R_4 + R_5 + R_6 + R_7 + R_8 + R_9 + R_{10} + R_{11} + R_{12} + R_{13} + R_{14} + R_{15} + R_{16}.$$

By use of these 16 rate equations, Eq. [11] can be converted to Eq. [12] as follows:

$$\frac{d[HY]}{dt} = R_9 + R_{10} + R_{12} + R_{14} - R_2 - R_4 - R_6 - R_8$$

$$\frac{d[HY]}{dt} = \left(R \cdot \frac{[CH_4][DY]}{[CH_{4in}][DY_{in}]} + R \cdot \frac{3}{4} \frac{[CH_3D][DY]}{[CH_{4in}][DY_{in}]} + R \cdot \frac{1}{2} \frac{[CH_2D_2][DY]}{[CH_{4in}][DY_{in}]} + R \cdot \frac{1}{4} \frac{[CHD_3][DY]}{[CH_{4in}][DY_{in}]} - R \cdot \frac{1}{4} \frac{[CH_3D][HY]}{[CH_{4in}][DY_{in}]} - R \cdot \frac{1}{2} \frac{[CH_2D_2][HY]}{[CH_{4in}][DY_{in}]} - R \cdot \frac{3}{4} \frac{[CHD_3][HY]}{[CH_{4in}][DY_{in}]} - R \cdot \frac{[CD_4][HY]}{[CH_{4in}][DY_{in}]} \right)$$

$$\frac{d[HY]}{dt} = \frac{R}{[CH_{4in}][DY_{in}]} \left([CH_4][DY] + \tfrac{3}{4}[CH_3D][DY] + \tfrac{1}{2}[CH_2D_2][DY] + \tfrac{1}{4}[CHD_3][DY] - \tfrac{1}{4}[CH_3D][HY] - \tfrac{1}{2}[CH_2D_2][HY] - \tfrac{3}{4}[CHD_3][HY] - [CD_4][HY] \right)$$

$$\frac{d[HY]}{dt} = \frac{R \cdot (4[CH_{4in}] + [DY_{in}])}{[CH_{4in}][DY_{in}]} \left(\frac{[CH_4][DY]}{(4[CH_{4in}] + [DY_{in}])} + \frac{3}{4} \frac{[CH_3D][DY]}{(4[CH_{4in}] + [DY_{in}])} + \frac{1}{2} \frac{[CH_2D_2][DY]}{(4[CH_{4in}] + [DY_{in}])} + \frac{1}{4} \frac{[CHD_3][DY]}{(4[CH_{4in}] + [DY_{in}])} - \frac{1}{4} \frac{[CH_3D][HY]}{(4[CH_{4in}] + [DY_{in}])} - \frac{1}{2} \frac{[CH_2D_2][HY]}{(4[CH_{4in}] + [DY_{in}])} - \frac{3}{4} \frac{[CHD_3][HY]}{(4[CH_{4in}] + [DY_{in}))} - \frac{[CD_4][HY]}{(4[CH_{4in}] + [DY_{in}])} \right)$$

$$\frac{d[HY]}{dt} = R \cdot \frac{4[CH_{4in}] + [DY_{in}]}{[DY_{in}]} \frac{1}{[CH_{4in}]} \cdot \left(\frac{(4[CH_4] + 3[CH_3D] + 2[CH_2D_2] + [CHD_3])[DY]}{4(4[CH_{4in}] + [DY_{in}])} - \frac{([CH_3D] + 2[CH_2D_2] + 3[CHD_3] + 4[CD_4])[HY]}{4(4[CH_{4in}] + [DY_{in}])} \right)$$

$$\frac{d[HY]}{dt} = R \cdot \frac{4[CH_{4in}] + [DY_{in}]}{[DY_{in}]} \cdot \left(\frac{(4[CH_{4in}] - [HY])[DY]}{4[CH_{4in}](4[CH_{4in}] + [DY_{in}])} - \frac{[HY][HY]}{4[CH_{4in}](4[CH_{4in}] + [DY_{in}])} \right)$$

$$\frac{d[HY]}{dt} = R \cdot \frac{4[CH_{4in}] + [DY_{in}]}{[DY_{in}]} \cdot \left(\frac{(4[CH_{4in}] - [HY])([DY_{in}] - [HY])}{4[CH_{4in}](4[CH_{4in}] + [DY_{in}])} - \frac{[HY][HY]}{4[CH_{4in}](4[CH_{4in}] + [DY_{in}])} \right)$$

$$\frac{d[HY]}{dt} = R \cdot \frac{4[CH_{4in}] + [DY_{in}]}{[DY_{in}]} \left(\frac{4[CH_{4in}][DY_{in}]}{4[CH_{4in}](4[CH_{4in}] + [DY_{in}])} - \frac{[HY][DY_{in}]}{4[CH_{4in}](4[CH_{4in}] + [DY_{in}])} - \frac{4[CH_{4in}][HY]}{4[CH_{4in}](4[CH_{4in}] + [DY_{in}])} + \frac{[HY][HY]}{4[CH_{4in}](4[CH_{4in}] + [DY_{in}])} - \frac{[HY][HY]}{4[CH_{4in}](4[CH_{4in}] + [DY_{in}])} \right)$$

$$\frac{d[HY]}{dt} = R \cdot \frac{4[CH_{4in}] + [DY_{in}]}{[DY_{in}]} \left(\frac{4[CH_{4in}][DY_{in}]}{4[CH_{4in}](4[CH_{4in}] + [DY_{in}])} - \frac{[HY](4[CH_{4in}] + [DY_{in}])}{4[CH_{4in}](4[CH_{4in}] + [DY_{in}])} \right)$$

$$\frac{d([HY]/4[CH_{4in}])}{dt} = R \cdot \frac{1}{4[CH_{4in}]} \cdot \frac{4[CH_{4in}] + [DY_{in}]}{[DY_{in}]} \cdot \left(\frac{[DY_{in}]}{4[CH_{4in}] + [DY_{in}]} - \frac{[HY]}{4[CH_{4in}]} \right).$$

ACKNOWLEDGMENTS

We thank J. P. Verduijn and Exxon Chemical Europe for supplying the Y2 sample. B.S. is indebted to the Flemish IWT for a Ph. D. fellowship. This work was financially supported by the Flemish government in the frame of the Geconcerteerde Onderzoeksactie (GOA). Discussions with B. Wouters and P. Grobet are highly appreciated.

REFERENCES

1. Kramer, G. J., van Santen, R. A., Emeis, C. A., and Nowak, A. K., *Nature* **363**, 529 (1993).
2. Jacobs, P. A., and Uytterhoeven, J. B., *J. Chem. Soc. Faraday Trans. 1* **69**, 359 (1973).
3. Van Santen, R. A., and Kramer, G. J., *Chem. Rev.* **95**, 637 (1995).
4. Van Santen, R. A., *in* "Advanced Zeolite Science and Applications" (J. C. Jansen, M. Stöcker, H. G. Karge, and J. Weitkamp, Eds.), Stud. Surf. Sci. Catal. Vol. 85, p. 273. Elsevier Science, Amsterdam, 1994.
5. Mikovsky, R. J., and Marshall, J. F., *J. Catal.* **44**, 170 (1976).
6. Dempsey, E., *J. Catal.* **39**, 155 (1975).
7. Jacobs, P. A., and Mortier, W. J., *Zeolites* **2**, 226 (1982).
8. Freude, D., Hunger, M., Pfeifer, H., and Schwieger, W., *Chem. Phys. Lett.* **128**, 62 (1986).
9. Sohn, J. R., DeCanio, S. J., Fritz, P. O., and Lunsford, J. H., *J. Phys. Chem.* **90**, 4847 (1986).
10. Rhodes, N. P., Rudham, R., and Stanbridge, N. H. J., *J. Chem. Soc. Faraday Trans.* **92**, 2817 (1996).
11. Haag, W. O., Lago, R. M., and Weisz, P. B., *Nature* **309**, 589 (1984).
12. Engelhardt, J., and Hall, W. K., *J. Catal.* **151**, 1 (1995).
13. Narbeshuber, T. F., Stockenhuber, M., Brait, A., Seshan, K., and Lercher, J. A., *J. Catal.* **160**, 183 (1996).
14. Mota, C. J. A., Menenzes, S. C., Nogueira, L., and Kover, W. B., *Appl. Catal. A* **146**, 181 (1996).
15. Iglesia, E., and Baumgartner, J. E., *Catal. Lett.* **21**, 55 (1993).
16. Chen, L., Lin, L., Xu, Z., Zhang, T., Liang, D., Xin, Q., and Ying, P., *Catal. Lett.* **35**, 245 (1995).
17. Larson, J. G., and Hall, K., *J. Phys. Chem.* **69**, 3080 (1965).
18. Sommer, J., Habermacher, D., Hachoumy, M., Jost, R., and Reynaud, A., *Appl. Catal. A* **146**, 193 (1996).
19. Sommer, J., Hachoumy, M., and Garin, F., *J. Am. Chem. Soc.* **116**, 5491 (1994).
20. Mota, C. J. A., Nogueira, L., and Kover, W. B., *J. Am. Chem. Soc.* **114**, 1121 (1992).
21. Mota, C. J. A., Martins, R. L., Nogueira, L., and Kover, W. B., *J. Chem. Soc. Faraday Trans.* **90**, 2297 (1994).
22. Haag, W. O., and Dessau, R. M., *in* "Proceedings, 8th International Congress on Catalysis, Berlin, 1984," Vol. 2, p. 305. Dechema, Frankfurt-am-Main, 1984.
23. Lercher, J. A., van Santen, R. A., and Vinek, H., *Catal. Lett.* **27**, 91 (1994).
24. Blaszkowski, S. R., Jansen, A. P. J., Nascimento, M. A. C., and van Santen, R. A., *J. Phys. Chem.* **98**, 12938 (1994).
25. Evleth, E. M., Kassab, E., and Sierra, L. R., *J. Phys. Chem.* **98**, 1421 (1994).
26. Kramer, G. J., and van Santen, R. A., *J. Am. Chem. Soc.* **117**, 1766 (1995).
27. Baekelandt, B. G., Janssens, G. O. A., Toufar, H., Mortier, W. J., Schoonheydt, R. A., and Nalewajski, R. F., *in* "Acidity and Basicity of Solids, Theory, Assessments and Utility" (J. Fraissard and L. Petrakis, Eds.), p. 95. Kluwer Academic, 1994.
28. Baekelandt, B. G., Janssens, G. O. A., Toufar, H., Mortier, W. J., Schoonheydt, R. A., and Nalewajski, R. F., *J. Phys. Chem.* **99**, 9784 (1995).
29. Janssens, G. O. A., Toufar, H., Baekelandt, B. G., Mortier, W., and Schoonheydt, R. A., *J. Phys. Chem.* **100**, 14443 (1996).
30. Janssens, G. O. A., Toufar, H., Baekelandt, B. G., Mortier, W., and Schoonheydt, R. A., *in* "Progress in Zeolite and Microporous Materials" (H. Chon, S.-K. Ihm, and Y. S. Uh, Eds.), Stud. Surf. Sci. Catal. Vol. 105, p. 725. Elsevier Science, Amsterdam, 1996.
31. Remy, M. J., Stanica, D., Poncelet, G., Feijen, E. J. P., Grobet, P. J., Martens, J. A., and Jacobs, P. A., *J. Phys. Chem.* **100**, 12440 (1996).
32. Barrer, R. M., and Sutherland, J. W., *Proc. R. Soc. A* **237**, 439 (1956).
33. Papp, H., Hinsen, W., Do, N. T., and Baerns, M., *Thermochim. Acta* **82**, 137 (1984).
34. Yashonath, S., Thomas, J. M., Nowak, A. K., and Cheetham, A. K., *Nature* **331**, 601 (1988).
35. Nulens, K., and Schoonheydt, R. A., unpublished results.
36. Meier, W. M., Olson, D. H., and Baerlocher, Ch., *Zeolites* **17** (1996).